Desalination and Water Treatment
www.deswater.com
doi: 10.5004/dwt.2021.26991

223 (2021) 335–349
May

Novel magnetically separable Ag@AgCl-Fe_3O_4/RGO nanocomposites for enhanced dielectric barrier discharge plasma reaction for high-performance water decontamination

Yongjun Shen[a,b,*,†], Yi Wang[b,†], Shuaikang Fang[b,†], Jae Kwang Park[c], Chao Pan[a], Yin Chen[b], Na Zhu[a,*], Huifang Wu[b,*]

[a]*Nantong University Xinglin College, Nantong 226008, China, Tel. +86 513 85012874; Fax: +86 513 85012856; emails: shenyj@ntu.edu.cn (Y. Shen), zhuna76418@163.com (N. Zhu)*
[b]*School of Chemistry and Chemical Engineering, Nantong University, Nantong 226019, China, email: 2437998491@qq.com (H. Wu)*
[c]*Department of Civil and Environmental Engineering, University of Wisconsin–Madison, 1415 Engineering Drive, Madison, WI 53706, USA*

Received 13 June 2020; Accepted 13 December 2020

ABSTRACT

A magnetic nanocatalyst, Ag@AgCl-Fe_3O_4/RGO, was prepared and used with dielectric barrier discharge plasma (DBD) to treat wastewater containing reactive black 5 azodye. Magnetic Fe_3O_4 and AgCl nanoparticles were successively loaded on reduced graphene oxide by hydrothermal and deposition–precipitation method, which was produced by restoring the graphene oxide. Ag nanoparticles were then photo-reduced on the surface of AgCl. The as-prepared nanoparticles were characterized by X-ray diffraction, scanning electron microscopy, Raman, and vibrating sample magnetometer analysis. Response surface methodology was used to optimize the preparation process of Ag@AgCl-Fe_3O_4/RGO nanoparticles and the decolorization of Reactive Black 5 in DBD-Ag@AgCl-Fe_3O_4/RGO combined system. The best material preparation conditions were that the dosage of Fe_3O_4/RGO, $AgNO_3$, NaCl, and the UV light reduction time are 110 mg, 0.23 g, 47 mg, and 1.1 h, respectively. The decolorization rate was measured by the absorbance before and after treatment, and the effects of the initial concentration, pH, conductivity, discharge current, and sodium dodecyl sulfonate concentration (SDS) in the dye solution were studied. The results showed that the optimum conditions for maximum Reactive Black 5 decolorization efficiency (99.3%) in the system of DBD-Ag@AgCl-Fe_3O_4/RGO were pH of 2, the concentration of 20 mg/L, the conductivity of 100 μS/cm, and do not add SDS, which was better than that of 88.6% in DBD alone. Meanwhile, the synthesis mechanism of Ag@AgCl-Fe_3O_4/RGO and the reaction mechanism of DBD-Ag@AgCl-Fe_3O_4/RGO were discussed. The morphology and repetition usage-ratio of the nanocatalyst was also studied during the treatment.

Keywords: Ag@AgCl-Fe_3O_4/RGO nanocatalyst; Dielectric barrier discharge; Response surface methodology; Reactive Black 5; Decolorization efficiency

1. Introduction

With the rapid development of petrochemical, pharmacy, pesticides, printing, and dyeing and leather processing industries, the discharge of large amounts of organic wastewater poses a serious threat to environmental safety and human health. Textile wastewater contains a high concentration of recalcitrant organic dyes and toxic intermediates, it is necessary to search for an effective method for eliminating dyes from wastewater economically and efficiently. Methods including adsorption [1,2], chemical coagulation processes [3], and biological treatment processes [4],

* Corresponding authors.

† These authors have contributed equally to this work and considered as co-first authors.

photocatalysis [5] were used. While these treatments own many typical drawbacks, such as time-consuming, inefficient, high cost, and easy to produce secondary pollution.

Recently, advanced oxidation processes (AOPs) [6–9] including Fenton, O_3, UV, and plasma have been widely used as a powerful alternative to treat water pollution. Among different classes of AOPs, a non-thermal plasma process (NTP) has attracted much attention due to its environmentally friendly nature and excellent oxidation properties. A large amount of activated species $^{\bullet}OH$, $^{\bullet}H$, $^{\bullet}O_2H$, and O_3 show a strong oxidizing ability during NTP, which can lead to both physical and chemical processes that directly or indirectly degrade different organic compounds rapidly and efficiently [10,11]. Dielectric barrier discharge (DBD) is considered as an effective discharge source for generating NTP owing to the advantages of stability of discharge, rich active substances, high efficiency, and high safety performance. However, this technology has disadvantages of low energy efficiency and mineralization, limiting a wide range of significant applications of DBD plasma technology. One of the ways to overcome these drawbacks is to combine DBD with nanocatalyst, which has been proved as an effective method. For instance, our previous research reported that better degradation efficiency could be obtained in the combination system of TiO_2 nanoparticles and DBD plasma [12]. Thus, it can be expected that excited-state conduction band electron and valence band hole pairs are generated by the cooperative reaction among TiO_2 and UV light irradiation, which are capable of initiating large quantities of oxidation and reduction reactions.

Among various kinds of materials, graphene has attracted public attention in recent years because of its excellent physical and chemical performances since it was discovered in 2004 [13]. Its conductivity and electromagnetic parameters of pure graphene are too high to satisfy the impedance matching, leading to strong reflection and weak absorption [14]. Thus, the properties of graphene oxide (GO) and reduced graphene oxide (RGO) can be better than graphene, making GO and RGO more easily assembled than other particles on the surface. Graphene oxide (GO) and RGO are known as 2D structures and have unique characteristics such as their functional electron absorption characteristics, low density, large surface area, and high conductivity [15]. Due to an extremely high specific surface area and unique two-dimensional structure, RGO is the best electromagnetic wave-absorbing material [16]. As a critical part of electromagnetic materials, ferrites are widely used due to their low cost, non-toxicity, and nice magnetic behavior. Among them, Fe_3O_4 is the most widely used magnetic nanoparticle. Recent research also shows that inorganic nanoparticles attached to graphene are effective in forming a novel graphene-based photocatalyst [17], which can make graphene own different characters, especially metal nanocrystal (such as Ag and Au). This metal nanocrystal is found to have a surface plasma resonance effect, which can be excited under UV light and perform a photocatalytic activity [18]. Recently, Ag@AgCl occurred into our eyesight, which was used as a co-catalyst to enhance the catalytic activity of semiconductors. A novel nanocatalyst Ag@AgCl-Fe_3O_4/RGO may be obtained while making Fe_3O_4 and Ag@AgCl loaded on the surface of RGO successively. Compared with the previous research of the TiO_2 nanocatalyst in conjunction with DBD plasma, the novel catalyst Ag@AgCl-Fe_3O_4/RGO can provide the advantage of UV light of DBD plasma for Ag@AgCl to produce holes–election pairs to form more active substances [19]. On the other hand, it can be easily recycled due to the presence of Fe_3O_4. In addition to the advantages of DBD, this combination may be a more effective way for pollutant remediation. To the best of our knowledge, the novel plasmonic nanocatalyst Ag@AgCl-Fe_3O_4/RGO has not yet been applied in degrading dye wastewater combined with DBD plasma. Therefore, this nanoparticle with DBD plasma was applied to wastewater treatment.

In addition, it is also essential to optimize the process variables for building an effective system on decolorization efficiency of dye wastewater. Therefore, the response surface methodology (RSM) [20] is often used to evaluate the individual and interaction effects among independent variables by the mathematical and statistical technique in the design of experiments. Yuliwati et al. [21] studied the relationship between four different process variables and response (outcomes of experiments) on the performances of modified polyvinylidene fluoride membranes by the approach of RSM.

In this paper, the objective was to seek a novel catalyst and then combine it with DBD plasma to achieve a better decolorization efficiency of Reactive Black 5 (RB 5), which was chosen as a model contaminant. Therefore, a novel plasmonic nanocatalyst of Ag@AgCl-Fe_3O_4/RGO was prepared by several modified methods. The optimal preparation conditions of Ag@AgCl-Fe_3O_4/RGO were determined from the model built by RSM according to the degradation efficiency of RB 5. The as-prepared catalysts were analyzed by X-ray diffraction (XRD), scanning electron microscopy (SEM), Raman, and vibrating sample magnetometer (VSM). Furthermore, RSM was also used to optimize the process of catalyst combined with DBD plasma. Meanwhile, the preparation mechanism of Ag@AgCl-Fe_3O_4/RGO and the synergistic mechanism of DBD-Ag@AgCl-Fe_3O_4/RGO were discussed. Finally, the repetition usage-ratio of Ag@AgCl-Fe_3O_4/RGO was researched as well combined with the morphology changes of nanocatalyst.

2. Experimental

2.1. Preparation of GO

All chemicals used in the experiments were of analytic grade. GO was prepared by a modified Hummers' method in this study [22]. A mixture of 0.5 g flake graphite (200 mesh, Nanjing Jicang Nanotechnology Co., Ltd., China) and 0.25 g $NaNO_3$ (Sinopharm Chemical Reagent Co., Ltd., China) was added into a three-necked flask in the low temperature cooling liquid circulating pump (DLSB-5/20, Zhengzhou Greatwall Scientific Industrial and Trade Co., Ltd., China) whose temperature had been cooled to 273–277 K and then 30 mL of concentrated H_2SO_4 (Sinopharm Chemical Reagent Co., Ltd., China) was added slowly into the three-necked flask. After the reaction time of 1 h, 0.3 g of $KMnO_4$ (Shantou Xilong Chemical Co., Ltd., China) was added to the three-necked flask at very

20 min and kept the reaction for 2 h. The resulting suspension was heated first to 308 K for 2 h and reacted with 60 mL deionized water up to 368 K for 30 min under the condition of stirring constantly. An aliquot of 20 mL of 30% H_2O_2 (Shanghai Jutai Special reagent Co., Ltd., China) was dropped into the suspension solution and stirred for 15 min. When the liquid suspension was cooled to room temperature, 10% HCl (Sinopharm Chemical Reagent Co., Ltd., China) and deionized water were used to wash the suspension by repeating centrifugation (Evolution RC, Kendro lab products Co., Ltd., America). Finally, the suspension was decanted slowly into the biofilm filtration until the sample was neutral and the stable GO solution was obtained.

2.2. Preparation of Fe_3O_4/RGO

In 80 mL of ethylene glycol solution (EG) (Shantou Xilong Chemical Co., Ltd., China), 40 mg of GO prepared above and 1 g of polyethylene glycol 4000 (Shanghai Richjoint Chemical Co., Ltd., China) weighed by an electronic analytical balance (Shanghai Hengping Scientific Instrument Co., Ltd., China) were uniformly dispersed by ultrasound (Kun Shan Ultrasonic Instruments Co., Ltd., China). Then, 0.27 g of $FeCl_3{\cdot}6H_2O$ (Shantou Xilong Chemical Co., Ltd., China) and 2 g NaAc (Shantou Xilong Chemical Co., Ltd., China) were added. After stirring completely, the mixture was transferred to a high temperature and high-pressure reaction kettle for 12 h under the temperature of 473 K. The suspension was dried after cooling to room temperature and washing by anhydrous ethanol (Sinopharm Chemical Reagent Co., Ltd., China) and deionized water. The final solid was Fe_3O_4/RGO.

2.3. Preparation of Ag@AgCl-Fe_3O_4/RGO

In 50 mL EG, 110 mg of the prepared Fe_3O_4/RGO was added and dispersed uniformly, followed by dissolving 0.23 g of $AgNO_3$ (Merck). Then, the suspension was decanted slowly into the three-necked flask, added dropwise with 10 mL of NaCl/EG (containing 47 mg NaCl) and stirred at a constant speed. The mixed solution was stirred for 15 h in a dark area. The samples were added to deionized water and exposed under 250 W UV light for 1.1 h. The sample Ag@AgCl-Fe_3O_4/RGO was obtained after desiccation at 323 K.

2.4. RB 5 degradation experiments

The RB 5 (Shanghai Jiaying Co., Ltd., China) was used as dye pollutants. The dye solution was prepared by RB 5 and deionized water. The pipette was used to remove 10 mL of 100 mg/L RB 5 dye solution into the reaction kettle of plasma device (Nanjing Suman Plasma Technology Co., Ltd., China). After switching on the power, adjust the input current and voltage to make the plate discharge. During the process of DBD and DBD-Ag@AgCl-Fe_3O_4/RGO systems, the effects of initial concentration, pH, conductivity, discharge current, and sodium dodecyl sulfonate concentration (SDS) content in the dye solution were investigated. NaOH (Shanghai Chemical Co., Ltd., China) or H_2SO_4 (Shantou Xilong Chemical Co., Ltd., China) was used to adjust pH to a target value. The whole discharge reaction time was 3 min. The samples were withdrawn from the reaction kettle and the removal of color was calculated by determining the absorbance of the dye solution at λ_{max} = 600 nm using a UV-vis spectrophotometer (752N, Shanghai Shunyu Hengping Technology Co., China). From these data, the apparent dye concentration is obtained and the decolorization efficiency (η, in %) was evaluated as follows:

$$\eta = \frac{C_0 - C_t}{C_0} \times 100\% \quad (1)$$

where C_0 and C_t are the absorbencies of the samples at time 0 and t, respectively.

All the experiments were conducted at least three times and the experimental data were the average of at least three measurements.

2.5. Characterization

XRD patterns were obtained on a D/MAX-IIIA X-ray diffractometer with Cu Kα radiation (λ = 0.154062 nm) over a 2θ range of 10°–80° with a scanning speed of 0.05°min^{-1}. After dried and ground into powder solid, Fe_3O_4/RGO, and Ag@AgCl-Fe_3O_4/RGO were placed on the sample platform and covered with a circle of 1 cm in diameter in order to measure the crystal structure of composites. Two kinds of samples were also spread evenly on the conductive adhesive and observed by the S-3000 N-type SEM at an accelerating voltage of 20 kV for observing the samples' morphology analysis. Raman spectroscopy was performed on P3000 with a suitable amount of solid samples dispersed in an aqueous solution. The catalyst Ag@AgCl-Fe_3O_4/RGO was also analyzed by a VSM for the analysis of the chemical state of typical elements and magnetic performance. The ultraviolet spectrophotometric (UV-vis) method is an analytic method of the material electron spectrum that was used to scan for the RB 5 solution in this study. The spectral wavelength ranged from 200 to 700 nm when radiation was absorbed by certain substance molecular.

3. Results and discussion

3.1. Formation process of Ag@AgCl-Fe_3O_4/RGO catalyst

The synthetic process of Ag@AgCl-Fe_3O_4/RGO catalyst is depicted in Fig. 1. The formation of Ag@AgCl-Fe_3O_4/RGO catalyst is explained below. The graphene oxide (GO) samples were oxidized from the graphene by a modified Hummers method. The surface of GO could be complexed Fe^{3+} and form Fe^{3+}-GO because a large amount of negative charge groups, such as hydroxyl groups (–OH), carboxyl groups (–COOH), and epoxies, distributed around the surface of GO [23]. In the reaction kettle, Fe_3O_4 nanoparticles, influencing the magnetic property and recycling of the material [16], were generated through a series of reactions as shown below.

$$Fe^{3+} + HOCH_2CH_2OH \rightarrow Fe^{2+} + CH_3CHO + H_2O \quad (2)$$

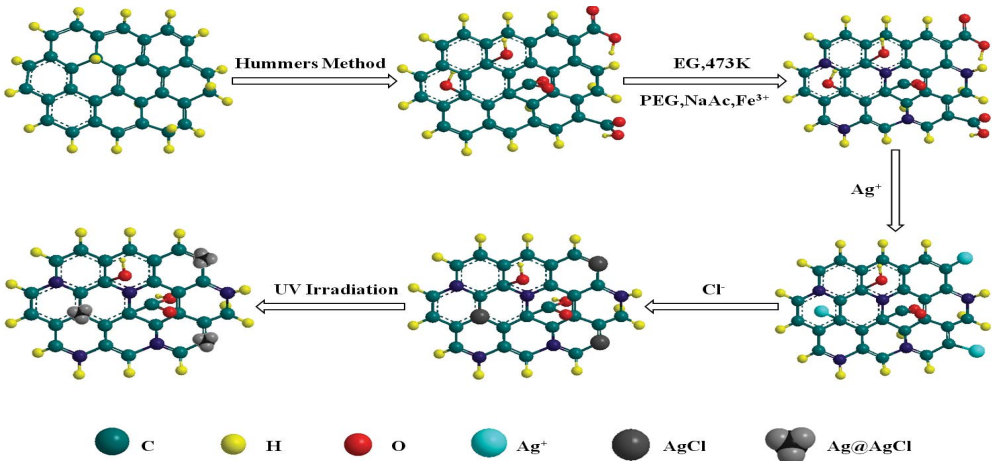

Fig. 1. Synthetic route of Ag@AgCl-Fe_3O_4/RGO.

$$Fe^{3+} + H_2O \rightarrow Fe(OH)_3 \quad (3)$$

$$Fe(OH)_3 + CH_3CHO \rightarrow CH_3COCOCH_3 + Fe(OH)_2 + H_2O \quad (4)$$

$$Fe(OH)_3 + Fe(OH)_2 \rightarrow Fe_3O_4 + H_2O \quad (5)$$

Fe_3O_4 was connected with graphene layers through the covalent bonds, which was one of the reasons that the Fe_3O_4 could spread evenly on the surface of the graphene layers. Meanwhile, the reductive aldehyde (CH_3CHO) produced in the reaction reduced the GO to the reduction of graphene oxide (RGO). However, GO was not restored entirely, still had parts of the active group and could be complexed with a part of Ag^+ to form Ag^+-RGO. Ag^+ produced by $AgNO_3$ could react with Cl^- produced by HCl, generating AgCl nanoparticles [24], which in turn was attached to the RGO sheets and connected with covalent bonds. Because of the existence of Fe_3O_4, the AgCl nanoparticles having cubic structures had been presented with irregular structural loading on the surface of RGO. Finally, a new plasmonic nanocatalyst of Ag@AgCl-Fe_3O_4/RGO was fabricated after using UV light to restore partial Ag of AgCl into Ag nanoparticles on the surface of AgCl nanoparticles, which was a medium to transfer the plasmon-induced electrons for AgCl to form active species [25].

3.2. Optimization on the preparation of Ag@AgCl-Fe_3O_4/RGO using RSM

3.2.1. Experimental design and analysis

The Box–Behnken experimental design (BBD) [26] was applied for investigating and validating the process variables that affected the catalytic performance of Ag@AgCl-Fe_3O_4/RGO on decolorization efficiency of RB 5. According to the preliminary experiments and analyses, there were some notices that needed to be taken into consideration during the experimental design of the optimization process. First, the dosage of Fe_3O_4/RGO as the principal subject determined the dosage of active points for the whole material. Second, the dosage of $AgNO_3$ was the only source of the silver element, determining the proportion of silver element in the whole material. Meanwhile, NaCl was the only source of chlorine element, determining the proportion of chlorine element in the whole material, and one of the vital raw materials for the synthesis of silver chloride [27]. Last, after preparation of the AgCl-Fe_3O_4/RGO nanoparticles, the UV photoreduction time was used in the formation process of Ag nanoparticles to form the final materials [18]. Therefore, the four critical variables influencing the performance of the catalyst, namely the dosages of Fe_3O_4/RGO (A), $AgNO_3$ (B), NaCl (C), and UV photoreduction time (D), were chosen as independent parameters and the decolorization efficiency of RB 5 (Y) was selected as the dependent response.

The experimental range and levels of independent factors for RB 5 decolorization were shown in Table 1. The program and experimental results of the BBD were given in Table 2 by using Design-Expert software (Company name, City, Country). Meanwhile, the regression model of Ag@AgCl-Fe_3O_4/RGO on the RB 5 decolorization efficiency was also proposed.

During the optimization process, a total of 29 experiments were performed in randomized order and a quadratic regression equation was built below as Eq. (6):

$$Y = 84.28 + 4.17A - 5.25B - 3.17C - 2.45D + 3.97AB - 1.45AC - 0.52AD - 3.25BC - 2.38AD - 1.95CD - 0.19A^2 - 0.92B^2 - 4.79C^2 - 2.29D^2 \quad (6)$$

Then, the rationality of the proposed model was verified by using the diagnostic checking tests that were provided across the analysis of variance (ANOVA) results shown in Table 3. The F-value of the model was 77.49, implying that the supposed model was significant for the decolorization of RB 5. The P-value was less than 0.05, indicating that the model is good [28]. Among the four variables, the dosage of $AgNO_3$ was most significant, followed by the dosage of Fe_3O_4/RGO (F = 214.78), the dosage of NaCl (F = 124.06), and the UV photoreduction time (F = 74.26). There were also interaction influences that occurred in four variables, especially significant between the dosage of Fe_3O_4/RGO and $AgNO_3$, the dosage of Fe_3O_4/RGO and NaCl due to their

Table 1
Factors and levels for Box–Behnken design

Variables	Symbols	Range and levels	
		Low (–1)	High (1)
Dosage of Fe_3O_4/RGO, mg	*A*	10	110
Dosage of $AgNO_3$, g	*B*	0.19	0.23
Dosage of NaCl, mg	*C*	40	80
UV photoreduction time, h	*D*	1	3

P-values were all less than 0.0001. In this study, the values of R^2 and R^2_{adj} were 0.987 and 0.975, respectively, and were all close to 1.0 which indicated that the model has a high fitting degree and feasibility [29]. Therefore, the optimal condition of decolorization efficiency on RB 5 could be optimized through the regression model obtained above.

3.2.2. Verification experiment

During the study of the interactions among four variables, a balance should be kept among them. Excess use of RGO may cause the waste of resources; thus, less dosage may provide less space for the other substances and was not lower conductivity to the application of wastewater treatment because of the stacked loading. A large amount of free Ag^+ could be formed while $AgNO_3$ was dissolved in the mixed solution. Once the dosage of Ag^+ was more than the optimal value, Fe_3O_4 nano-particles could not control the growth and distribution of AgCl particles on the surface of RGO. Meanwhile, if the dosage of $AgNO_3$ and NaCl increased beyond some optimal threshold value, most of Ag^+ would react with Cl^- in NaCl and then AgCl was formed beyond the maximum loading of the carrier, a factor clearly harmful to the catalyst performance [30]. In addition, due to the defects of AgCl which could be sensitive to the light, UV photoreduction could break down parts of AgCl to form nano-silver clusters adhering to the surface of AgCl [31]. Above all, an excellent photocatalyst material of Ag@AgCl-Fe_3O_4/RGO would be prepared on the premise that four variables take the appropriate values.

Through the Design Expert 8.0 software, the optimal conditions of the preparation of Ag@AgCl-Fe_3O_4/RGO, namely, the dosage of Fe_3O_4/RGO, $AgNO_3$, NaCl, and UV photoreduction time were 110 mg, 0.23 g, 47 mg, and 1.1 h, respectively. To test the predictability of the RSM model, the optimum preparation conditions were carried out treating the RB 5 dye wastewater and the predicted and actual values of decolorization efficiency were obtained as shown in Table 4. The deviation with the model prediction was only 1.3% which could indicate that the model supposed in this study on the optimization of the prepared materials Ag@AgCl-Fe_3O_4/RGO was predictable.

3.3. Characterization of Ag@AgCl-Fe_3O_4/RGO under optimal conditions

3.3.1. X-ray diffraction

The XRD patterns were measured to investigate the components and structure of Fe_3O_4/RGO and Ag@AgCl-Fe_3O_4/RGO materials, which are respectively shown in Figs. 2a and b. From Fig. 2, it is observed that the diffraction peaks at about 30.14°, 35.13°, 43.13°, 57.02°, and 62.52° were all identical to the indices d(220), d(311), d(400), d(511), and d(440) of Fe_3O_4 (JCPDS NO. 65-3107), respectively. In addition, the diffraction peaks at 2θ = 27.83°, 32.24°, 46.23°, 54.82°, 57.48°, 67.46°, and 76.73° also could be assigned to (111), (200), (311), (222), (400), (331), and (420) of the AgCl (JCPDS NO. 31-1238). The diffraction peaks at 38.12° and 77.472° were found as well, which corresponded to (111) and (311) of the Ag crystal. In addition, there was no obvious diffraction peak attributed to graphite observed, indicating that the stacking of RGO sheets remained disordered [32].

Table 2
Program and experimental results of the BBD

Run	*A*	*B*	*C*	*D*	Decolorization efficiency (η)	
					Actual (%)	Predicted (%)
1	110	80	0.21	2	79.4	88.2
2	60	60	0.21	2	85.2	88.6
3	10	60	0.21	3	75.7	69.8
4	110	60	0.19	2	89.3	86.1
5	10	60	0.21	1	79.9	80.9
6	60	60	0.21	2	83.1	78.4
7	10	60	0.23	2	70.4	79.9
8	10	40	0.21	2	75.7	69.6
9	60	80	0.21	1	78.8	79.6
10	10	80	0.21	2	73.0	88.9
11	60	60	0.19	1	86.3	75.7
12	60	40	0.23	2	79.8	83.0
13	60	80	0.21	3	70.2	83.7
14	60	40	0.21	3	80.8	79.7
15	110	40	0.21	2	87.9	83.9
16	110	60	0.21	1	88.2	66.9
17	60	40	0.19	2	83.3	76.8
18	60	60	0.21	2	84.3	88.1
19	110	60	0.21	3	81.9	73.4
20	10	60	0.19	2	88.8	78.8
21	60	60	0.23	3	70.5	86.4
22	60	60	0.21	2	85.5	80.6
23	60	80	0.19	2	83.1	86.2
24	110	60	0.23	2	86.8	71.0
25	60	60	0.21	2	83.3	84.3
26	60	40	0.21	1	81.6	84.3
27	60	60	0.19	3	86.3	84.3
28	60	80	0.23	2	66.6	84.3
29	60	60	0.23	1	80.0	84.3

3.3.2. Raman

Fig. 3 shows the Raman spectra of (a) Fe_3O_4/RGO and (b) Ag@AgCl-Fe_3O_4/RGO, both of which can clearly find the two adsorption peaks of RGO, namely the D and G

Table 3
ANOVA of decolorization efficiency for RB 5

Source	Sum of squares	Degree of freedom	Mean square	*F*-value	*P*-value	
Model	1,052.27	14	75.16	77.49	<0.0001	Significant
A	208.33	1	208.33	214.78	<0.0001	Significant
B	330.75	1	330.75	340.99	<0.0001	Significant
C	120.33	1	120.33	124.06	<0.0001	Significant
D	72.03	1	72.03	74.26	<0.0001	Significant
AB	63.20	1	63.20	65.16	<0.0001	Significant
AC	8.41	1	8.41	8.67	0.0107	
AD	1.10	1	1.10	1.14	0.3044	
BC	42.25	1	42.25	43.56	<0.0001	Significant
BD	22.56	1	22.56	23.26	0.0003	
CD	15.21	1	15.21	15.68	0.0014	
A^2	0.24	1	0.24	0.25	0.6234	
B^2	5.48	1	5.48	5.65	0.0323	
C^2	149.09	1	149.09	153.70	<0.0001	Significant
D^2	34.14	1	34.14	35.20	<0.0001	Significant
Residual	13.58	14	0.97			
Lack of fit	8.89	10	0.89	0.76	0.6719	
Pure error	4.69	4	1.17			
Cor. total	1,065.85	28				

$R^2 = 0.987$; $R^2_{adj} = 0.975$.

Table 4
Response optimization

Dosage of Fe_3O_4/RGO (*A*, mg)	110
Dosage of $AgNO_3$ (*B*, g)	0.23
Dosage of NaCl (*C*, mg)	47
UV photoreduction time (*D*, h)	1.1
Decolorization efficiency (η)	
Predicted (%)	91.0
Actual (%)	89.7

band. D band at 1,348 cm^{-1} corresponded to the vibration of sp3 carbon atoms of disordered graphite which proved that the absence of defects in the graphene structure [33]. G band at 1,592 cm^{-1} was due to the vibrations of sp2 carbon atoms in a 2D hexagonal lattice [34]. Therefore, the intensity ratio between the D and G band (ID/IG) was used to determine the disorder of graphene and its loading catalyst [35].

From Fig. 3 and Table 5, it can be found that the ID/IG value of Ag@AgCl-Fe_3O_4/RGO was obviously smaller than that of Fe_3O_4/RGO, indicating that the disorder of the catalyst Ag@AgCl-Fe_3O_4/RGO was bigger than that of Fe_3O_4/RGO. There were two reasons for this phenomenon. First, reduction reaction would happen to remove part of oxygen-containing groups and destroy the C=C structure which could change the hybridization of sp2 to sp3 when adding the AgCl on the Fe_3O_4/RGO and the light

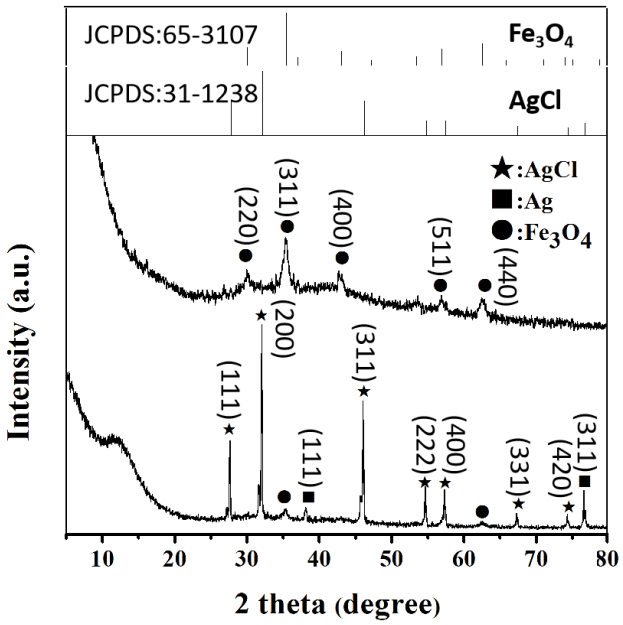

Fig. 2. XRD patterns of samples: (a) Fe_3O_4/RGO and (b) Ag@AgCl-Fe_3O_4/RGO.

reduction process of AgCl-Fe_3O_4/RGO. This may lead to the increase of ID/IG and disorder of graphene and its loading catalyst. Second, the Ag@AgCl loaded on the surface of the precursors Fe_3O_4/RGO which made the vacancy of carbon atoms decreased and the disorder increased.

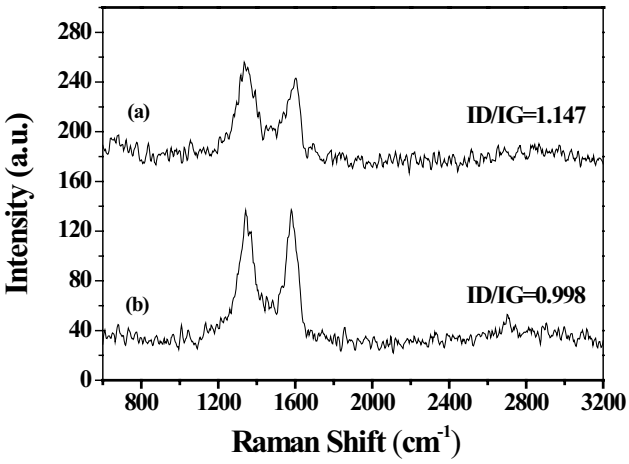

Fig. 3. Raman spectra of samples: (a) Ag@AgCl-Fe_3O_4/RGO and (b) Fe_3O_4/RGO.

Table 5
I_D/I_G of Fe_3O_4/RGO and Ag@AgCl-Fe_3O_4/RGO

Samples	Fe_3O_4/RGO	Ag@AgCl-Fe_3O_4/RGO
ω_D (cm^{-1})	1,342	1,335
ω_G (cm^{-1})	1,579	1,604
I_D/I_G	0.998	1.147

3.3.3. Scanning electron microscopy

Figs. 4a and b are the SEM images of two materials Fe_3O_4/RGO and Ag@AgCl-Fe_3O_4/RGO. It can be seen from Fig. 4a that RGO was a thin layer with wrinkles and Fe_3O_4 nanoparticles were spherical and uniformly distributed on the surface of the RGO, although there was also a little reunion. As shown in Fig. 4b, a large number of small particles attached to the surface of AgCl particles which could be analyzed as Ag nanoparticles combined with the result of XRD. It could be proved that Ag@AgCl particles had been generated in the material. Combined with the images of XRD and SEM, Ag@AgCl-Fe_3O_4/RGO photocatalytic material had been successfully prepared.

3.3.4. Vibrating sample magnetometer

The magnetic property of the Ag@AgCl-Fe_3O_4/RGO photocatalytic material was investigated by VSM at room temperature with an applied field of –20,000 to 20,000 Oe. The saturation magnetization and residual magnetization of Ag@AgCl-Fe_3O_4/RGO could be obtained from Fig. 5. As shown in Fig. 5, there was no hysteresis loop on the magnetic hysteresis loop of the prepared nanoparticles, which meant that the residual magnetization was almost zero, indicating that the Ag@AgCl-Fe_3O_4/RGO samples had a superparamagnetic behavior. The saturation magnetization of the sample (6.17 emu/g) is significantly smaller than that of Fe_3O_4 particles prepared by the hydrothermal method (47.78 emu/g), and it is also less than the saturation magnetization of Fe_3O_4/RGO (42.39 emu/g) [36], which could be attributed to the introduction of Ag@AgCl and RGO, indexing that the magnetic properties of the prepared materials could be changed by adjusting the ratio of metal salts to GO [37]. Due to the superparamagnetism of the Ag@AgCl-Fe_3O_4/RGO catalyst, this study used this feature to separate the catalyst from the wastewater and realize the recycling of the catalyst, thereby increasing the competitiveness of catalyst in industrial application.

3.4. Decolorization analysis of RB 5 by DBD-Ag@AgCl-Fe_3O_4/RGO

3.4.1. Effect of initial concentration

The effect of initial concentration was evaluated over the range of 20–100 mg/L. As shown in Fig. 6a, the initial concentration of dye solution of RB 5 had a significant effect on the decolorization efficiency when the operating conditions were voltage of 70 V, discharge current of 1.1 A, pH of 6, the conductivity of 100 μS/cm, and dosage of the catalyst of 0.5 g/L. It could be found that higher decolorization efficiency would be obtained under lower initial concentration. At the reaction time of 120 s, the

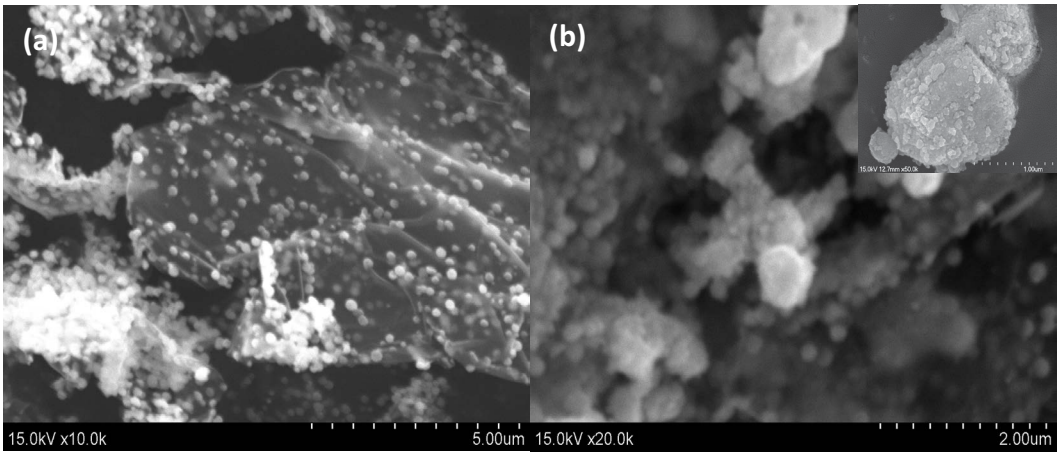

Fig. 4. SEM images of samples: (a) Fe_3O_4/RGO and (b) Ag@AgCl-Fe_3O_4/RGO.

decolorization efficiency of the initial concentration of 20 mg/L was 8.9% higher than that of 100 mg/L.

The quantity of the active substance was similar under the same operating conditions, which played a decisive role on the decolorization efficiency of dye wastewater. Therefore, a high initial concentration of RB 5 obtained a bad decolorization efficiency compared with the low one. It could also be explained that the increase of the initial concentration of RB 5 would lead to the competition adsorption among RB 5 molecules because the adsorption capacity of RB 5 using the catalyst of Ag@AgCl-Fe_3O_4/RGO was limited [38].

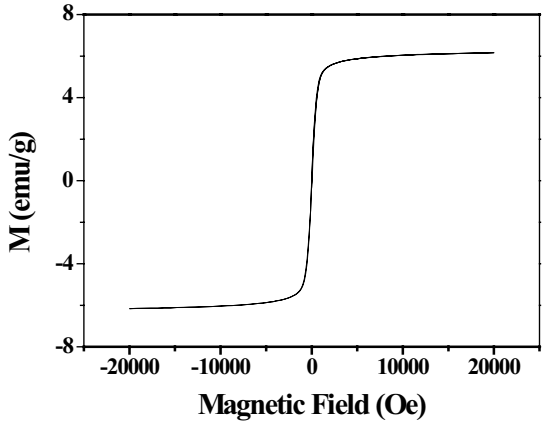

Fig. 5. Magnetic hysteresis diagram of the sample Ag@AgCl-Fe_3O_4/RGO.

3.4.2. Effect of initial pH

For a heterogeneous medium, the active sites on the surface of most semiconductors depend on the concentration of hydrogen ions (H^+) or hydroxide ions (OH^-) in an aqueous solution. Therefore, the pH value of the reaction solution is a vital factor in the adsorption property and catalytic activity of the photocatalyst [39]. In order to investigate the effect of initial pH, the influence of different initial pH ranged from 2 to 12 on the decolorization efficiency of RB 5 wastewater was studied. Fig. 6b shows the results of the decolorization efficiency at different pH values and indicated that the decolorization efficiency on RB 5 decreased by increasing the pH values, namely lower pH values, were beneficial to the decolorization of dye wastewater in DBD system.

The reason for this phenomenon was that the acid environment could guarantee the hydroxyl radicals (•OH) and other active substances with strong oxidation ability. In the alkaline environment, organic pollutants could not spread to the atmosphere in the form of CO_2 after being oxidized but produced CO_3^{2-} or HCO_3^- which could react with the hydroxyl radicals (•OH) in the wastewater. Due to the reduction of hydroxyl radicals (•OH) in the wastewater,

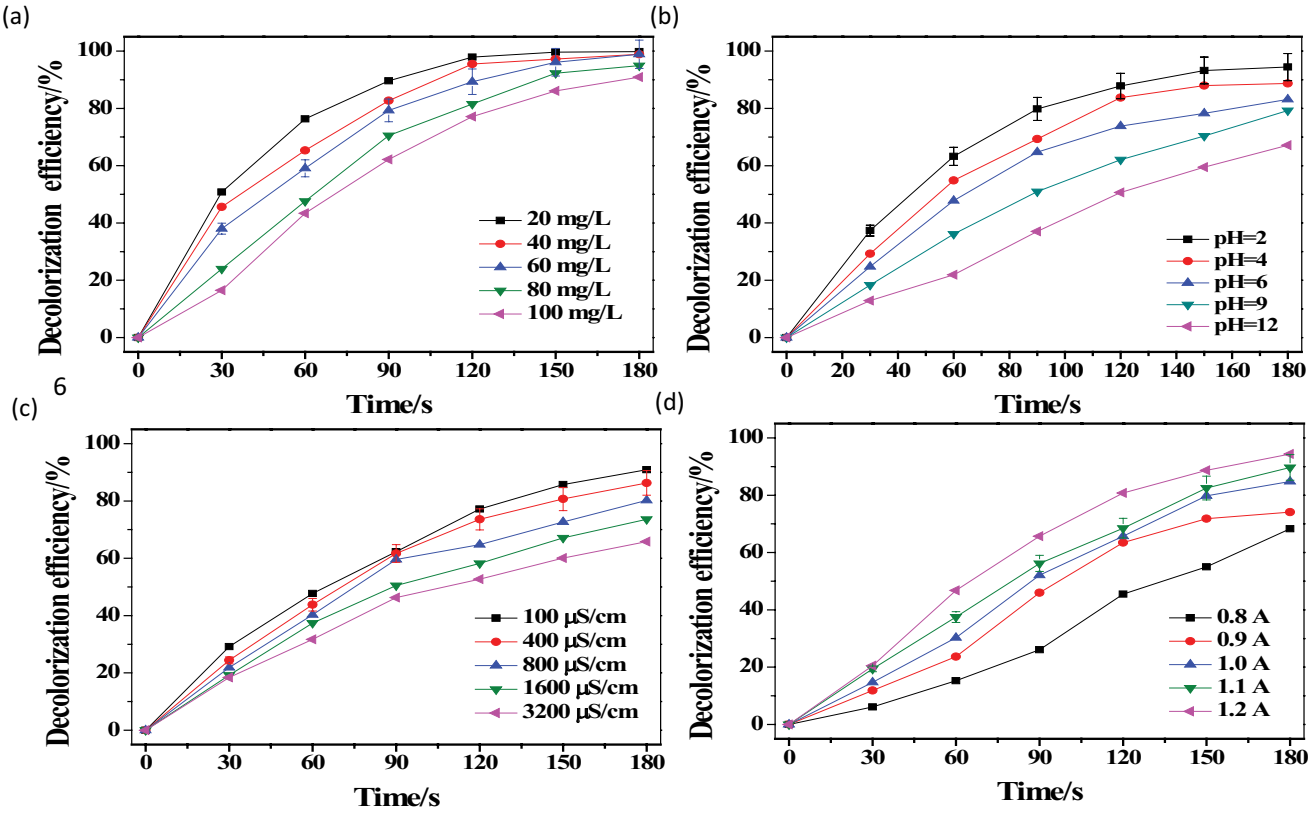

Fig. 6. Effect of (a) initial concentration, (b) initial pH, (c) conductivity, and (d) discharge current on decolorization efficiency of RB 5.

the decolorization efficiency on RB 5 decreased sharply. From another point of view, the chromophoric group of the dye molecules would be damaged when the ozone produced from the high-pressure discharge directly reacted with the organic pollutants under the acid environment, resulting in the dye wastewater decolorization. Therefore, the key on decolorizing of RB 5, a sort of azo dyestuff, was to break down the major chromophoric group of RB 5, namely the azo double bond. The azo bond was not stable and easy to be damaged under acid conditions. There is a large number of H^+ in strongly acidic wastewater which could inhibit the H_2O_2 decomposition of the whole system and further was conductive to the decolorization process of the wastewater. Working at alkaline pH was not beneficial to the dye decolorization because the reaction between H^+ and OH^- accelerated the decomposition of H_2O_2 [40]. To sum up, a better degradation efficiency of wastewater could be obtained when the high-energy electrons emitted by DBD plasma collided with the dye molecules under acidic pH.

3.4.3. Effect of conductivity

The conductivity of the reaction solution was the concentration of electrolyte in the dye solution and adjusted by the saturated solution of KCl. The effect of initial conductivity of dye RB 5 ranged from 100 to 3,200 μS/cm was studied on the decolorization efficiency under the other conditions that were the voltage of 70 V, discharge current of 1.1 A, pH of 6, initial concentration of 100 mg/L, and dosage of the catalyst of 0.5 g/L. Fig. 6 shows that the decolorization efficiency decreased by increasing the initial conductivity of the RB 5 solution, which revealed that increasing the initial conductivity was not conductive to the color removal of dye in the DBD-Ag@AgCl-Fe_3O_4/RGO system.

Due to the high initial conductivity of the RB 5 solution, various ions (K^+, Cl^-) in the reaction solution would have directional movement and form the current under the action of the applied electric field, making the system frequent leakage of electricity, and which reduced the discharge effect of the transient breakdown. Then, the formation of active substances such as $^{\bullet}OH$, O_3, and H_2O_2 decreased obviously which directly lead to the decrease of decolorization efficiency.

3.4.4. Effect of discharge current

Fig. 6d shows the effect of discharge current on the decolorization efficiency of RB 5 dye solution when the voltage, discharge current, pH, initial concentration, and dosage of catalyst were 70 V, 1.1 A, 6, 100 mg/L, and 0.5 g/L, respectively. The conclusion can be drawn from Fig. 6d that the decolorization efficiency of RB 5 increased by increasing the discharge current. The discharge current was a key parameter in plasma since it regulates the amount of oxidizing species produced. More active substances were produced and the UV intensity increased at high discharge current, which played a significant role in the decolorization process. If the discharge current was too small, the system would not normally work to produce the active substances. But the energy would be wasted if increasing the value of discharge current blindly. Therefore, optimal operating conditions need to be determined during lots of experiments and association with the actual situation.

3.5. Optimization analysis on the degradation of RB 5 in the system of DBD-Ag@AgCl-Fe_3O_4/RGO by using RSM

3.5.1. Experimental design and analysis

In this chapter, the BBD was used to optimize the decolorization of RB 5 in the system of DBD-Ag@AgCl-Fe_3O_4/RGO. A total of 29 experiments were conducted in this optimization design mode. During the experimental design, the decolorization efficiency of RB 5 (Y') was chosen as dependent response and the four critical variables in DBD-Ag@AgCl-Fe_3O_4/RGO system, namely the initial concentration (A'), initial pH (B'), dosage of catalyst (C'), and discharge current (D'), were selected as independent parameters. The experimental range and levels of independent factors for RB 5 decolorization in DBD-Ag@AgCl-Fe_3O_4/RGO were shown in Table 6.

The program of the BBD was given in Table 7 by using Design-Expert software. According to the conditions of each group, the experiments were performed and the regression model of DBD-Ag@AgCl-Fe_3O_4/RGO on the RB 5 decolorization efficiency was also proposed. Meanwhile, a quadratic regression equation between dye decolorization rate (Y') and four variables were established below as Eq. (7):

$$Y' = 89.44 - 3.77A' - 1.12B' - 1.13C' + 1.31D' - 0.15A'B' - 0.025A'C' + 0.6A'D' - 0.93B'C' - 1.47C'D' + 1.94A'^2 + 3.34B'^2 + 1.86C'^2 + 2.09D'^2 \quad (7)$$

Table 8 shown the ANOVA results of the proposed model, and the P-value was less than 0.0001 which meant the supposed model was significant for the decolorization of RB 5. From Table 8, it can be found that the effect of the initial concentration was the most marked and other variables in the order of the effect on decolorization of RB 5 were initial pH (F = 58.73), discharge current (F = 52.82), and dosage of catalyst (F = 46.55). The synergistic effect of B'-initial pH and C'-discharge current was significant with $p < 0.05$. Meanwhile, the values of R^2 and R^2_{adj} were 0.986 and 0.973, respectively, and all close to 1.0 which indicated that the model has a high fitting degree and feasibility. Therefore, the model could be used to optimize the decolorization efficiency of RB 5 in DBD-Ag@AgCl-Fe_3O_4/RGO system.

3.5.2. Response surface analysis of interaction factors on the decolorization efficiency of RB 5 by DBD-Ag@AgCl-Fe_3O_4/RGO

Fig. 7 presents the contour plot and 3D response surface which demonstrated the effect of four variables on the degradation efficiency of RB 5 in the combined system of DBD-Ag@AgCl-Fe_3O_4/RGO.

The combined effects of initial concentration and pH on decolorization efficiency of RB5 are shown in Fig. 7I. Under the predefined conditions, the system generated the same amount of active species, so the decolorization rate would be faster at low concentrations. Meanwhile, the

Table 6
Factors and levels for Box–Behnken design

Variables	Symbols	Range and levels	
		Low (–1)	High (1)
Initial concentration (mg/L)	A'	60	100
Initial (pH)	B'	2	6
Dosage of catalyst (mg)	C'	3	7
Discharge current (A)	D'	1.0	1.2

Table 7
Program and experimental results of the BBD

Run	A'	B'	C'	D'	Decolorization efficiency (η)	
					Actual (%)	Predicted (%)
1	80	4	5	1.1	89.2	89.4
2	80	6	5	1.2	93.7	94.9
3	60	4	3	1.1	98.3	98.3
4	100	4	7	1.1	88.1	88.3
5	80	4	5	1.1	89.6	89.4
6	60	4	7	1.1	96.1	95.9
7	100	2	5	1.1	92.5	92.3
8	100	6	5	1.1	89.9	89.4
9	80	4	7	1.2	91.9	91.9
10	80	2	3	1.1	95.7	96.1
11	80	6	3	1.1	95.4	95.4
12	60	4	5	1	96.3	96.7
13	80	4	3	1.2	98.1	97.5
14	100	4	5	1.2	91.8	91.4
15	60	4	5	1.2	98.6	98.1
16	80	4	5	1.1	89.2	89.4
17	100	4	3	1.1	90.1	90.5
18	60	2	5	1.1	99.3	99.6
19	80	2	5	1	95.8	94.9
20	80	4	3	1	92.0	91.8
21	80	4	5	1.1	89.7	89.4
22	80	4	7	1	92.3	92.7
23	80	6	7	1.1	91.7	91.3
24	80	2	5	1.2	97.1	97.5
25	80	4	5	1.1	89.5	89.4
26	100	4	5	1	87.5	88.0
27	60	6	5	1.1	97.3	97.4
28	80	2	7	1.1	95.7	95.7
29	80	6	5	1	92.6	92.4

azo groups of RB 5 were unstable under the conditions of strong acid and easy to be destroyed by the active species, which were produced by plasma and had strong activity and oxidation ability. In addition, the decolorization efficiency was particularly controlled by the concentration of dye wastewater as detailed above, whereas initial pH was less important, which was in line with the variance analysis results.

As seen in Fig. 7II, high decolorization efficiency was obtained at low values of initial concentration and dosage of catalyst. The decolorization efficiency of RB 5 decreased by increasing the dosage of catalyst. This may be contributed to the fact that the increase of the catalyst dosage decreased the transmittance of the whole wastewater solution, making the catalyst not absorbed the UV light entirely which was not conductive to the decolorization efficiency of RB 5. Thus, a conclusion also could be made that the effect of initial concentration was more important than that of the dosage of catalyst, which was in line with the variance analysis results.

A phenomenon was found from Fig. 7III that the high decolorization efficiency would be obtained at a low initial concentration and high discharge current. Firstly, with the increase of the initial concentration of RB 5, the radicals provided for the decolorization had approached to the saturated levels and could not be enough for the reaction [41]. Secondly, the discharge current played an important role in producing the active substances, thereby the decolorization efficiency increased by increasing the discharge current. But it would cause resources to be wasted when blindly increased the discharge current.

Under the initial concentration of 80 mg/L and discharge current of 1.1 A, the decolorization efficiency of RB 5 decreased as the dosage of catalyst increased when the initial pH kept invariable from Fig. 7IV. When the pH was low (2–3), the decomposition rate of H_2O_2 increased slowly. Meanwhile, the appropriate dosage of catalyst could not make agglomeration of catalyst which affected the normal operation of experiments. Thus, the effect of initial pH on the decolorization efficiency of RB 5 was more significant than that of the dosage of catalyst.

The three-dimensional response surface plots were the graphical representations of the regression equation. The main purpose of the response surface was to effectively track the optimal value of the variable to maximize the response. As seen in Fig. 7V, the optimal decolorization efficiency was obtained when the initial pH and discharge current were 2 and 1.2 A, respectively. A conclusion could be made that the effect of initial pH on the decolorization process of RB 5 was more significant than that of the discharge current because the former was greater than the latter, which was consistent with the previous variance analysis.

It still could be found from Fig. 7VI that the better decolorization efficiency occurred in a low dosage of catalyst and high value of discharge current. The effect of discharge current on the decolorization efficiency of RB 5 in the system of DBD-Ag@AgCl-Fe_3O_4/RGO was more significant than that of the dosage of catalyst.

3.5.3. Verification experiment

The optimal operating conditions of the decolorization efficiency on RB 5 in DBD-Ag@AgCl-Fe_3O_4/RGO system were selected through the Design Expert 8.0 software and shown in Table 9, namely, the initial concentration, initial pH, dosage of catalyst, and discharge current were 60 mg/L, 2, 3 mg, and 1.2 A, respectively. In order to test the predictability of the RSM model, the optimum conditions were used to treat the RB 5 dye wastewater. The predicted and

Table 8
ANOVA of discoloration efficiency for RB 5

Source	Sum of squares	Degree of freedom	Mean square	*F*-value	*P*-value	
Model	344.74	14	24.62	72.23	<0.0001	Significant
A′	176.33	1	176.33	517.23	<0.0001	Significant
B′	20.02	1	20.02	58.73	<0.0001	Significant
C′	15.87	1	15.87	46.55	<0.0001	Significant
D′	18.01	1	18.01	52.82	<0.0001	Significant
A′B′	0.090	1	0.090	0.26	0.6154	
A′C′	1.000E-002	1	1.000E-002	0.029	0.8665	
A′D′	1.00	1	1.00	2.93	0.1088	
B′C′	3.42	1	3.42	10.04	0.0068	
B′D′	1.000E-002	1	1.000E-002	0.029	0.8665	
C′D′	10.56	1	10.56	30.98	<0.0001	Significant
A'^2	24.16	1	24.16	70.87	<0.0001	Significant
B'^2	70.32	1	70.32	206.26	<0.0001	Significant
C'^2	22.93	1	22.93	67.25	<0.0001	Significant
D^2	30.47	1	30.47	89.39	<0.0001	Significant
Residual	4.77	14	0.34			
Lack of fit	4.56	10	0.46	8.61	0.0263	
Pure error	0.21	4	0.053			
Cor. total	349.51	28				

$R^2 = 0.986$; $R^2_{adj} = 0.973$.

actual values of the decolorization efficiency are summarized in Table 9. The deviation with the model prediction was only 0.4%, demonstrating that the model supposed in this study on the optimization by DBD-Ag@AgCl-Fe_3O_4/RGO was predictable.

Then, a series of experiments were further performed under the above operating conditions between DBD alone and DBD-Ag@AgCl-Fe_3O_4/RGO system. The decolorization efficiencies of the two systems were 88.6% and 99.3%, respectively, which indicated that the system of DBD-Ag@AgCl-Fe_3O_4/RGO for dye wastewater treatment was better than that of the DBD alone.

3.6. Synergistic mechanism of DBD-Ag@AgCl-Fe_3O_4/RGO

Synergistic mechanism of DBD-Ag@AgCl-Fe_3O_4/RGO is shown in Fig. 8. In the process of DBD on the decolorization efficiency of RB 5, large amounts of high-energy electron produced by high voltage alternating current could bombard and collide with water molecules, which were excited and ionized to produce excitation molecules, ions, and secondary electron, producing lots of active substances such as O_3, –OH, and hyperoxy radicals ($O_2^{\bullet-}$). Then, the organic dye molecules reacted with these active substances and then were broken down into small molecules, achieving the aim of decolorization.

The Ag@AgCl nanoparticles were excited under illumination of UV light produced from the DBD system. Then, the plasma oscillation occurred on the surface electron and generated electron–hole pairs. Under the electric field, free-electron appears to be broken away from their nuclei and transferred on the surface of Ag, reducing O_2 into $O_2^{\bullet-}$, while the holes transferred on the surface of AgCl and oxidized H_2O into $^{\bullet}OH$ [42]. Due to these active substances, the dye molecules could be degraded into small molecules.

In addition, dye molecules could be enriched on the surface of graphene because of its large specific area. The RB 5 molecules were concentrated on the graphene layers and inclined to Ag@AgCl nanoparticles, through noncovalent π–π intermolecular interactions between graphene and dye molecules [43]. Then, the active substances could react with the pollutant molecules, improving the utilization rate of –OH and holes and thereby increasing the decolorization efficiency of RB 5 in the system of DBD-Ag@AgCl-Fe_3O_4/RGO. Therefore, in the whole system, the synergistic effect between DBD and photocatalysts decolorized the organic dye molecules, achieving the aim of synergistic degradation.

3.7. Repetition usage-ratio of Ag@AgCl-Fe_3O_4/RGO materials

Fig. 9 indicates the repetition usage-ratio of Ag@AgCl-Fe_3O_4/RGO nanoparticles on the decolorization efficiency of RB 5 dye wastewater in the DBD plasma system. As could be seen from Fig. 9, the decolorization efficiency only changed about 5% after using the Ag@AgCl-Fe_3O_4/RGO catalyst for 5 times. The changes of catalyst Ag@AgCl-Fe_3O_4/RGO before and after being used were shown in Fig. 10. It could be found that large amounts of silver clusters attached to the surface of the catalyst before treatment, while parts of them fell off after 5 times treatments. This may be the reason for the decreasing of decolorization efficiency of RB 5 after using the catalyst for five times.

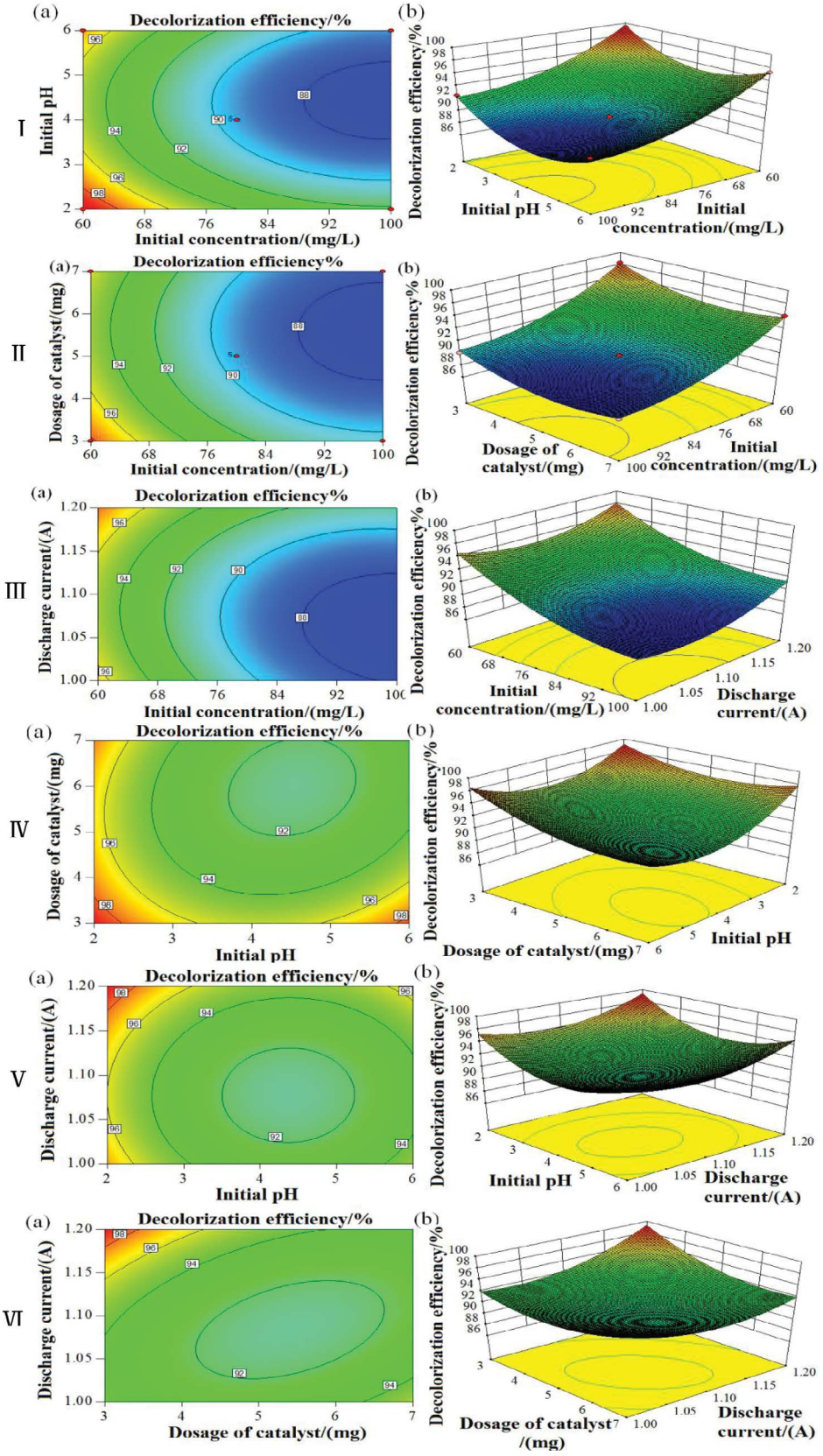

Fig. 7. Combined effects of four variables on decolorization efficiency (%): (a) contour plot and (b) response surface. (I) initial concentration and initial pH, (II) initial concentration and the dosage of catalyst, (III) initial concentration and discharge current, (IV) initial pH and the dosage of catalyst, (V) initial pH and discharge current, and (VI) dosage of catalyst and discharge current.

Table 9
Response optimization

Initial concentration (*A*, mg/L)	Initial pH (*B*)	Dosage of catalyst (*C*, mg)	Discharge current (*D*, A)	Decolorization efficiency (%)	
				Predicted (%)	Actual (%)
60	2	3	1.2	99.7	99.3

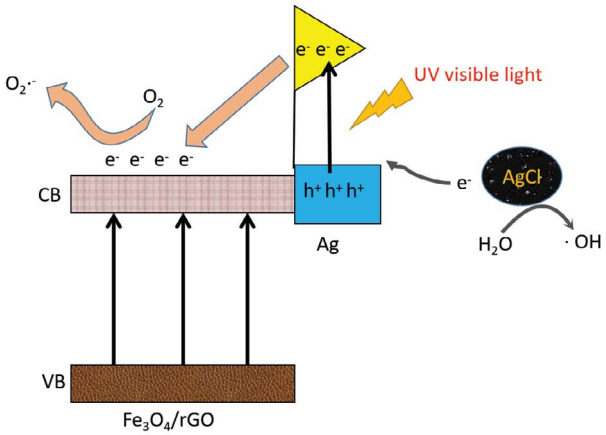

Fig. 8. Synergistic mechanism of DBD-Ag@AgCl-Fe_3O_4/RGO.

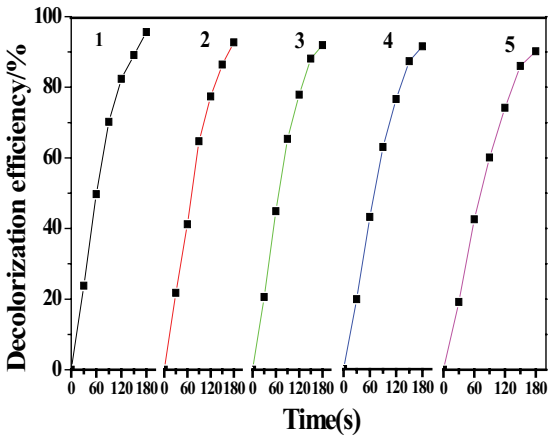

Fig. 9. Repetition usage-ratio of Ag@AgCl-Fe_3O_4/RGO.

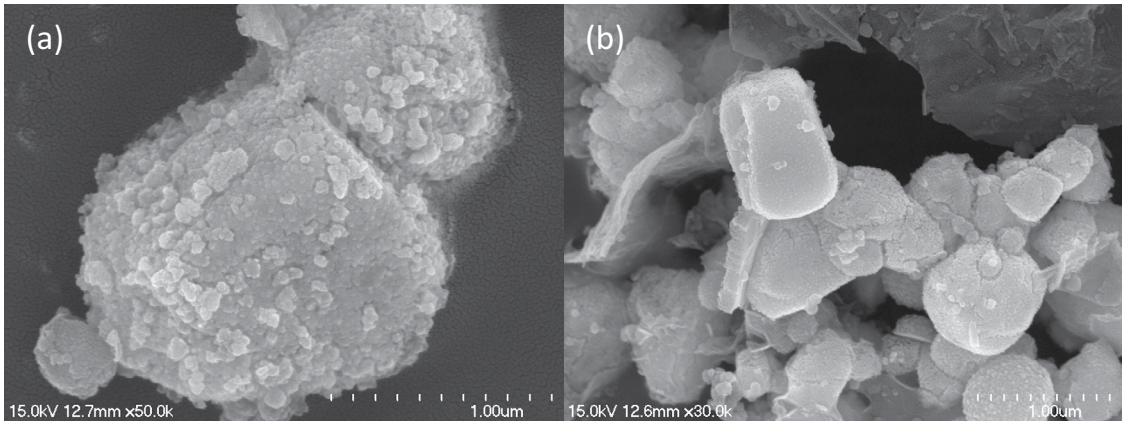

Fig. 10. Comparison before and after treatment of Ag@AgCl-Fe_3O_4/RGO: (a) before and (b) after treatment.

Compared with the catalyst in the industrial application which could only use for two times, the nanoparticles Ag@AgCl-Fe_3O_4/RGO can be used repeatedly. The high decolorization efficiency could still be obtained under the use of Ag@AgCl-Fe_3O_4/RGO catalyst for five times through the repetition usage-ratio and morphology analysis. The stability of the material, according to our experiment on the repeated use rate of the material, it can be seen that after 5 cycles of use, the dehydration rate changes only by 5%. Therefore, the material has excellent stability.

4. Conclusion

The Ag@AgCl-Fe_3O_4/RGO nanoparticle was prepared by the hydrothermal method, deposition–precipitation method, and photoreduction method, and analyzed by XRD, SEM, Raman, and VSM. These analyses were all indicated that the as-prepared nanoparticles were successful. The optimum conditions of the Ag@AgCl-Fe_3O_4/RGO preparation, namely, the dosages of Fe_3O_4/RGO, $AgNO_3$, NaCl, and UV photoreduction time optimized by RSM were 110 mg, 0.23 g, 47 mg, and 1.1 h, respectively. Then, the nanoparticle was used in decolorizing the RB 5 dye wastewater combined with DBD. By validating the effects of four variables on RB 5 decolorization efficiency, the results showed that the optimal operating conditions were the initial concentration of 60 mg/L, initial pH of 2, the dosage of the catalyst of 3 mg, and discharge current of 1.2 A. The most marked effect on the decolorization efficiency was the initial concentration, followed by initial pH, discharge current, and dosage of

catalyst. Under the optimal operating conditions above, the decolorization efficiency reached 99.3% in the DBD-Ag@AgCl-Fe_3O_4/RGO system compared with that of 88.6% in DBD alone. In addition, the preparation mechanism of Ag@AgCl-Fe_3O_4/RGO materials and the synergistic mechanism of DBD-Ag@AgCl-Fe_3O_4/RGO were also studied. Finally, Ag@AgCl-Fe_3O_4/RGO materials were found to be reused for five times. Therefore, the combination of Ag@AgCl-Fe_3O_4/RGO and DBD plasma has been proved to be an efficient method for RB 5 wastewater degradation.

Acknowledgments

The authors gratefully acknowledge the financial support from the National Natural Science Foundation of China (no. 21246010) and Nantong University Xinglin College Natural Science (no. 2018K115).

References

[1] R. Liu, H. Liu, Z. Xu, J. Qu, R. Zhang, Treatment of dye wastewater with permanganate oxidation and in situ formed manganese dioxides adsorption: cation blue as model pollutant, J. Hazard. Mater., 176 (2010) 926–931.
[2] B.P. Bastakoti, Y.Q. Li, M. Imura, Polymeric micelle assembly with inorganic nanosheets for construction of mesoporous architectures with crystallized walls, Angew. Chem. Int. Ed., 54 (2015) 4222–4225.
[3] O. Lefebvre, R. Moletta, Treatment of organic pollution in industrial saline wastewater: a literature review, Water Res., 40 (2006) 3671–3682.
[4] O. Türgay, G. Ersöz, S. Atalay, J. Forss, U. Welander, The treatment of azo dyes found in textile industry wastewater by anaerobic biological method and chemical oxidation, Sep. Purif. Technol., 79 (2011) 26–33.
[5] G.W. Pan, X.H. Jing, X.Y. Ding, Y.J. Shen, S.J. Xu, W.J. Miao, Synergistic effects of photocatalytic and electrocatalytic oxidation based on a three-dimensional electrode reactor toward degradation of dyes in wastewater, J. Alloys Compd., 809 (2019), doi: 10.1016/j.jallcom.2019.151749.
[6] I. Oller, S. Malato, J.A. Sánchez-Pérez, Combination of advanced oxidation processes and biological treatments for wastewater decontamination-a review, Sci. Total Environ., 409 (2011) 4141–4166.
[7] S. Papic, D. Vujevic, N. Koprivanac, D. Šinko, Decolourization and mineralization of commercial reactive dyes by using homogeneous and heterogeneous Fenton and UV/Fenton processes, J. Hazard. Mater., 164 (2009) 1137–1145.
[8] P. Colindres, H. Yee-Madeira, E. Reguera, Removal of Reactive Black 5 from aqueous solution by ozone for water reuse in textile dyeing processes, Desalination, 258 (2010) 154–158.
[9] Y. Shen, Q. Xu, J. Liang, W. Xu, Degradation of Reactive Yellow X-RG by O_3/Fenton system: response surface approach, reaction mechanism, and degradation pathway, Water Sci. Technol., 74 (2016) 2483–2496.
[10] J. Feng, R. Liu, P. Chen, S. Yuan, D. Zhao, J. Zhang, Z. Zheng, Degradation of aqueous 3,4-dichloroaniline by a novel dielectric barrier discharge plasma reactor, Sci. Pollut. Res., 22 (2015) 4447–4459.
[11] Y. Shen, L. Lei, X. Zhang, M. Zhou, Y. Zhang, Effect of various gases and chemical catalysts on phenol degradation pathways by pulsed electrical discharges, J. Hazard. Mater., 150 (2008) 713–722.
[12] Y. Shen, S. Han, Q. Xu, Y. Wang, Z. Xu, B. Zhao, R. Zhang, Optimizing degradation of Reactive Yellow 176 by dielectric barrier discharge plasma combined with TiO_2 nano-particles prepared using response surface methodology, J. Taiwan Inst. Chem. Eng., 60 (2016) 302–312.
[13] K.S. Novoselov, A.K. Geim, S.V. Morozov, D. Jiang, Y. Zhang, S.V. Dubonos, I.V. Grigorieva, A.A. Firsov, Electric field effect in atomically thin carbon films, Science, 306 (2004) 666–669.
[14] L. Kong, X. Yin, Y. Zhang, X. Yuan, Q.F. Ye, L. Cheng, L. Zhang, Electromagnetic wave absorption properties of reduced graphene oxide modified by maghemite colloidal nanoparticle clusters, J. Phys. Chem. C, 117 (2013) 19701–19711.
[15] M.A. Baghchesara, H.R. Azimi, A.G. Shiravizadeh, Improving the intrinsic properties of rGO sheets by S-doping and the effects of rGO improvements on the photocatalytic performance of Cu_3Se_2/rGO nanocomposites, Appl. Surf. Sci., 466 (2019) 401–410.
[16] J. Luo, S. Pan, Y. Wei, C. Jiang, J. Xu, Synthesis, characterization, and microwave absorption properties of reduced graphene oxide/strontium ferrite/polyaniline nanocomposites, Nanoscale Res. Lett., 11 (2016), doi: 10.1186/s11671-016-1340-x.
[17] P.K. Boruah, B. Sharma, I. Karbhal, M.V. Shelke, M.R. Das, Ammonia-modified graphene sheets decorated with magnetic Fe_3O_4 nanoparticles for the photocatalytic and photo-Fenton degradation of phenolic compounds under sunlight irradiation, J. Hazard. Mater., 325 (2016) 90–100.
[18] J. Zhou, Y. Cheng, J. Yu, Preparation and characterization of visible-light-driven plasmonic photocatalyst Ag/AgCl/TiO_2 nanocomposite thin films, J. Photochem. Photobiol., A, 223 (2011) 82–87.
[19] Y. Bao, K. Chen, AgCl/Ag/g-C_3N_4 hybrid composites: preparation, visible light-driven photocatalytic activity and mechanism, Nano-Micro Lett., 8 (2016) 182–192.
[20] Y.J. Shen, Q.H. Xu, D.D. Gao, Degradation of an anthraquinone dye by ozone/Fenton: response surface approach and degradation pathway, Ozone Sci. Eng., 39 (2017) 219–232.
[21] E. Yuliwati, A.F. Ismail, W.J. Lau, B.C. Ng, A. Mataram, M.A. Kassim, Effects of process conditions in submerged ultrafiltration for refinery wastewater treatment: optimization of operating process by response surface methodology, Desalination, 287 (2012) 350–361.
[22] J. Wu, X. Shen, L. Jiang, K. Wang, K. Chen, Solvothermal synthesis and characterization of sandwich-like graphene/ZnO nanocomposites, Appl. Surf. Sci., 256 (2010) 2826–2830.
[23] X. Shen, J. Wu, S. Bai, H. Zhou, One-pot solvothermal syntheses and magnetic properties of graphene-based magnetic nanocomposites, J. Alloys Compd., 506 (2010) 136–140.
[24] Y. Li, J. Zheng, Q. Sheng, B. Wang, Synthesis of Ag@AgCl nanoboxes, and their application to electrochemical sensing of hydrogen peroxide at very low potential, Microchim. Acta, 182 (2015) 61–68.
[25] C. An, S. Peng, Y. Sun, Facile synthesis of sunlight-driven AgCl:Ag plasmonic nanophotocatalyst, Adv. Mater., 22 (2010) 2570–2574.
[26] P. Sharma, L. Singh, N. Dilbaghi, Optimization of process variables for decolorization of Disperse Yellow 211 by *Bacillus subtilis* using Box-Behnken design, J. Hazard. Mater., 164 (2009) 1024–1029.
[27] Y. Tang, Z. Jiang, G. Xing, A. Li, P. Kanhere, Y. Zhang, T. Sum, S. Li, X. Chen, Z. Dong, Efficient Ag@AgCl cubic cage photocatalysts profit from ultrafast plasmon-induced electron transfer processes, Adv. Funct. Mater., 23 (2013) 2932–2940.
[28] S.S. Moghaddam, M. Moghaddam, M. Arami, Coagulation/flocculation process for dye removal using sludge from water treatment plant: optimization through response surface methodology, J. Hazard. Mater., 175 (2010) 651–657.
[29] B. Kayan, B. Gözmen, Degradation of Acid Red 274 using H_2O_2 in subcritical water: application of response surface methodology, J. Hazard. Mater., 201 (2011) 100–106.
[30] H. Yu, C.J. Miller, A. Ikeda-Ohno, T.D. Waite, Photodegradation of contaminants using Ag@AgCl/rGO assemblages: possibilities and limitations, Catal. Today, 224 (2014) 122–121.
[31] P. Wang, B. Huang, X. Qin, X. Zhang, Y. Dai, J. Wei, M.H. Whangbo, Ag@AgCl: a highly efficient and stable photocatalyst active under visible light, Angew. Chem. Int. Ed., 47 (2008) 7931–7933.

[32] D. Sun, Q. Zou, Y. Wang, Y. Wang, W. Jiang, F. Li, Controllable synthesis of porous Fe_3O_4@ZnO sphere decorated graphene for extraordinary electromagnetic wave absorption, Nanoscale, 6 (2014) 6557–6562.
[33] Z. Zhu, X. Sun, G. Li, H. Xue, H. Guo, X. Fan, X. Pan, J. He, Microwave-assisted synthesis of graphene-Ni composites with enhanced microwave absorption properties in Ku-band, J. Magn. Magn. Mater., 377 (2015) 95–103.
[34] W. Chen, S. Li, C. Chen, L. Yan, Self-assembly and embedding of nanoparticles by in situ reduced graphene for preparation of a 3D graphene/nanoparticle aerogel, Adv. Mater., 23 (2011) 5679–5683.
[35] A.C. Ferrari, D.M. Basko, Raman spectroscopy as a versatile tool for studying the properties of graphene, Nat. Nanotechnol., 8 (2013) 235–246.
[36] M.K. Zheng, X.G. Ma, J. Hu, X.X. Zhang, D. Li, W.Y. Duan, Novel recyclable BiOBr/Fe_3O_4/RGO composites with remarkable visible-light photocatalytic activity, RSC Adv., 10 (2020) 19961–19973.
[37] G. Liu, W. Jiang, Y. Wang, S. Zhong, D. Sun, J. Liu, F. Li, One-pot synthesis of Ag@Fe_3O_4/reduced graphene oxide composite with excellent electromagnetic absorption properties, Ceram. Int., 41 (2015) 4982–4988.
[38] M. Bhaumik, A. Maity, V.K. Gupta, Synthesis and characterization of Fe^0/TiO_2 nano-composites for ultrasound assisted enhanced catalytic degradation of reactive black 5 in aqueous solutions, J. Colloid Interface Sci., 506 (2017) 403–414.
[39] C. Pei, W. Chu, The photocatalyic degradation and modeling of 2,4-Dichlorophenoxyacetic acid by bismuth tungstate/peroxide, Chem. Eng. J., 223 (2013) 665–669.
[40] E. Basturk, M. Karatas, Advanced oxidation of Reactive Blue 181 solution: a comparison between Fenton and Sono-Fenton process, Ultrason. Sonochem., 21 (2014) 1881–1885.
[41] Y.J. Shen, Q.H. Xu, R.R. Wei, Mechanism and dynamic study of reactive red X-3B dye degradation by ultrasonic-assisted ozone oxidation process, Ultrason. Sonochem., 38 (2017) 681–692.
[42] H. Zhang, X. Fan, X. Quan, S. Chen, H. Yu, Graphene sheets grafted Ag@AgCl hybrid with enhanced plasmonic photocatalytic activity under visible light, Environ. Sci. Technol., 45 (2011) 5731–5736.
[43] M. Zhu, P. Chen, M. Liu, Graphene oxide enwrapped Ag/AgX (X = Br, Cl) nanocomposite as a highly efficient visible-light plasmonic photocatalyst, ACS Nano, 5 (2011) 4529–4536.